

# Fiber-Optic Silicon Fabry-Perot Interferometric Bolometer: The Influence of Mechanical Vibration and Magnetic Field

Qiwen Sheng, Guigen Liu, Nezam Uddin, Matthew L. Reinke, and Ming Han

**Abstract**—Plasma radiation plays an important role in the operation and control of magnetic confinement fusion and is typically measured by bolometers. Here, we study the influence of mechanical vibration and magnetic field, which are typically present in magnetic confinement fusion devices, on the performance of a fiber-optic bolometer (FOB) based on silicon Fabry-Perot interferometer (FPI) demodulated by a scanning diode laser. It is found that both the vibration and magnetic field could cause large noise due to the birefringence of the silicon FPI. To mitigate the birefringence effects, we demonstrated two effective methods: polarization maintaining FOB and polarization scrambling. We show that two methods can be effective in mitigating the effect caused by the sensor birefringence: (1) replacing the regular single-mode fiber in the FOB system with polarization-maintaining fiber and (2) using a polarization scrambler after the laser source. For both methods, no significant increase in the noise was observed in the vibration and magnetic field tests. Our research highlights the importance of the polarization management for the FOB systems toward their practical applications in magnetic-confinement fusion systems.

**Index Terms**—Optical fiber sensors, Bolometers, Plasma applications, Fabry-Perot interferometer, Birefringence, Temperature measurement.

## I. INTRODUCTION

IN magnetically confined fusion (MCF) devices, measurement of plasma radiation is essential in the understanding and control of plasma [1]. Plasma radiation covers a broad spectral range from soft X-ray to UV and is typically measured by bolometers which infers the radiation power flux from the temperature rise of an absorber [2]. Resistive bolometers are the most widely used bolometers and have been extensively studied for plasma diagnosis in the tokamak and the helical devices [1-3]. The noise equivalent power density (NEPD) is a critical parameter to evaluate the performance of the bolometer. Recently, a bolometer utilizing a Pt absorber attached on a SiN insulator with a Pt resistor demonstrated a noise equivalent power density (NEPD) of 0.2 W/m<sup>2</sup> [3]. Though, the resistive bolometers have shown

excellent NEPD performance in controlled environments, their performance experiences unavoidable degradation due to the strong electromagnetic interference (EMI) present in magnetically confined fusion systems. Alternatively, infrared video bolometer (IRVB) has been reported which records the temperature rise of a thin metallic foil via an infrared video camera, giving rise to a 2D image of the plasma radiation profile [4]. Although a benchtop NEPD value as low as 0.23 W/m<sup>2</sup> has been reported [4], the NEPD of IRVBs is, in general, larger than resistive bolometers. In addition, IRVBs require the infrared camera to have direct optical access to the foil, which may limit their applications in fusion systems. In general, deployment of bolometric sensors on MCF devices is constrained by thermal and mechanical requirements, which motivates innovations to reach smaller size and higher temperature limits, even at increased NEPD, in order to have sufficient coverage to enable tomographic inversion.

The limitations of resistive bolometers and IRVBs motivated us to develop fiber-optic bolometers (FOBs) that have many advantages such as immunity to EMI, light weight, and small size [5-7]. Previously, we demonstrated an FOB based on a high-finesse silicon Fabry-Perot interferometer (FPI) fabricated on regular single-mode fiber (SMF) [5, 7], in which the silicon FPI serves as both the absorber and the temperature sensor. The FOB shows a temperature resolution of 0.12 mK and a NEPD value of 0.27 W/m<sup>2</sup> in the lab. The measured NEPD is comparable with resistive bolometers and IRVBs. Although the experimental results show that the FOB is promising for plasma applications, the NEPD was measured in a controlled environment free of mechanical vibration and strong static or quasi-static magnetic field, both of which can be present in a magnetic-confinement fusion system. In this paper, we study the influences of these parameters on the performance of FOBs and the mitigation of the influences. Specifically, based on an FOB that we demonstrated earlier [5], we characterized the noise performance of the FOB when the fiber with the bolometer was vibrated by an electromagnetic shaker. The experimental results showed that the vibration significantly increases the noise of the FOB system. We also characterized the effect on the performance of the FOB from quasi-dc magnetic field generated from a solenoid applied on the fiber. We found that the change of the magnetic field along the axial direction of the fiber also led to signal variations of the FOB. The sensitivity of the FOB to mechanical vibration and magnetic field can both be attributed to the birefringence of the

This work was supported by U.S. Department of Energy (DoE) DE-SC0019058; DE-AC05-00OR22725) (*Corresponding author: Ming Han.*)

Q. Sheng, G. Liu, N. Uddin, and M. Han are with Department of Electrical and Computer Engineering, Michigan State University, East Lansing, Michigan, 48840 USA. (e-mail: shengqiwen1988@gmail.com; guigenliu@hotmail.com; uddinnez@msu.edu; mhan@egr.msu.edu).

M. L. Reinke is with Oak Ridge National Laboratory, Oak Ridge, Tennessee, 37831, USA. (e-mail: reinkeml@ornl.gov)

silicon sensor head. It is known that both mechanical perturbation to the fiber and magnetic field (through Faraday rotation) can change the polarization state of light traveling in the fiber, which in turn leads to signal variations of the FOB due to the birefringence of the silicon FOB head. We show that two methods can be effective in mitigating the effect caused by the sensor birefringence: (1) replacing the regular SMF in the FOB with polarization-maintaining (PM) fiber and (2) using a polarization scrambler after the laser source. For both methods, no significant increase in the noise was observed in the vibration and magnetic field tests. Our research highlights the importance of the polarization management for the FOB systems toward their practical applications in magnetic-confinement fusion systems. We also briefly make note of the ability to use the FOB or fiber-sensing to form dedicated measurements of what amounts to ‘polluting’ signals for a bolometer.

## II. FOB PREPARATION AND BIREFRINGENCE CHARACTERIZATION

### A. FOB Preparation

Figure 1(a) schematically shows the structure of the FOB head used in the study [5]. It consisted of a lead-in single-mode fiber (SMF), a small section of graded-index multimode optical fiber (GI-MMF) serving as a collimator [7], and a 75  $\mu\text{m}$  thick double-side polished silicon pillar attached to the end face of the GI-MMF collimator. The silicon pillar was coated with a high reflection (HR) dielectric thin film on the surface glued to the GI-MMF collimator and a 150-nm thick gold layer on the front surface, which form a high-finesse planar silicon FPI. The plasma radiation impinging onto the front surface increases the temperature of the silicon FPI, which is deduced by the fringe shift of reflection spectrum of the silicon FPI. The FOBs used in the experiment were fabricated following the process described in Ref. [5]. Figs. 1(b) and (c) show, respectively, a picture of a fabricated FOB head and its reflection spectrum measured by a white light source and an optical spectrum analyzer (OSA) with a spectral resolution of 20 pm. It shows

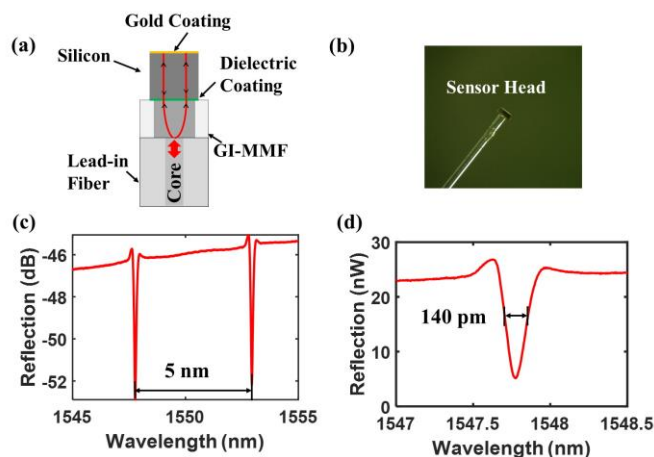


Fig. 1. (a) Schematic of the FOB head. (b) Side view of an FOB head. (c) Reflection spectrum of the FOB measured by an OSA. (d) Enlarged view of a spectral notch.

that the free spectrum range (FSR) of the FPI is 5 nm and the full-width at half-maxima (FWHM) of the resonant notch is 140 pm, corresponding to a finesse of 35 for the FPI. Two ‘bumps’ are found on the shoulders of the resonant notches with the one on the shorter-wavelength side is more prominent, as shown more clearly in Fig. 1 (d). These bumps are believed to arise from the imperfect parallelism of the two surfaces of the FPI as well as the non-normal incidence of the light to the FPI [8]. They typically have little negative effect on the operation of the bolometer.

### B. FOB Birefringence Characterization

The birefringence of the silicon element in our FOB structure has been observed and studied. Although crystalline silicon has a cubic structure that should be optically isotropic, birefringence may be present in the silicon wafers used for FOB fabrication due to the thermal and elastic strains induced during the manufacturing of silicon wafers [9]. In our case, the processes involved in fabricating silicon pillars from the silicon wafers and depositing the multilayer dielectric film on the silicon pillar can also introduce strain to the silicon pillar, giving rise to additional birefringence to the FOB head.

The birefringence of the FOB head was characterized by looking at the responses, in terms of resonant wavelength shift ( $d\lambda$ ) and equivalent temperature change ( $dT$ ), of the FOB as the polarization of the source laser was changed, using an experiment setup schematically shown in Fig. 2. A distributed feedback (DFB) diode laser with a regular SMF pigtail that emits linearly polarized light around 1550 nm was used as the light source. The central wavelength of the DFB laser was tuned to be close to one of the resonances of the FOB by controlling the temperature of the DFB laser. Then, an external triangle current waveform was used to scan wavelength of the DFB laser with a frequency of 2 kHz over a wavelength range of 240 pm. Through a circulator (Circulator 1), the light from the DFB laser was directed to the FOB head (with  $\sim 1.5$  mW laser power reaching the FOB head) and the light reflected back by the FOB was received by a photodetector (PD). The signal from the PD was recorded using a data acquisition (DAQ) system with a sampling rate of 2 MHz. A mechanical polarization controller (PC) was placed after the Circulator 1 to manually adjust the polarization state of the light from the DFB

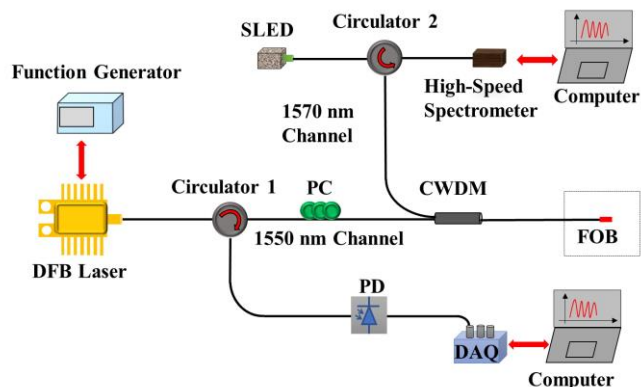


Fig. 2. Experimental setup to characterize the sensitivity of FOB to the light polarization variation.

injected into the FOB.

The FOB will respond to ambient temperature variations. In addition, the manual tuning of the PC may introduce variations of the laser power injected to the FOB and the gold mirror on the sensor head has a  $\sim 2\%$  absorption to the laser light, giving rise to potential temperature variations of the FOBs when the PC was tuned to alter the polarization. The responses of FOB to the ambient temperature change and the intensity variation are irrelevant to laser polarization and need to be separated from the overall response of the FOB. To measure the temperature variation arising from ambient temperature variations and the laser intensity variations, a white-light system, including a SLED source, another circulator (Circulator 2), and a high-speed spectrometer, was included in the system through a coarse wavelength division multiplexers (CWDM). The DFB laser used the 1550 nm channel of CWDM, while the white light system measured the reflection spectrum of the FOB over the 20 nm wavelength range of the 1570 nm channel of the CWDM. The transmission spectra of both DFB laser and the white light source after the CWDM are shown in Fig. 3(a). The power of the SLED that reach the FOB was on the order of 1 mW. Figure 3 (b) shows the reflection spectrum of the bolometer obtained by using the high-speed spectrometer. Apparently, the two interrogation systems were separated and independent. Note that the CWDM was placed after the PC so that the tuning of the PC would not affect either the polarization state or the power of the white-light source. As a result, any wavelength shift recorded by the white-light system is expected to be from the ambient temperature variations and/or the DFB laser power fluctuations. The wavelength shifts of the silicon FPI measured by both systems were converted to equivalent temperature changes using the coefficient of  $d\lambda/dT = 84.6$  pm/K reported in our previous work [10].

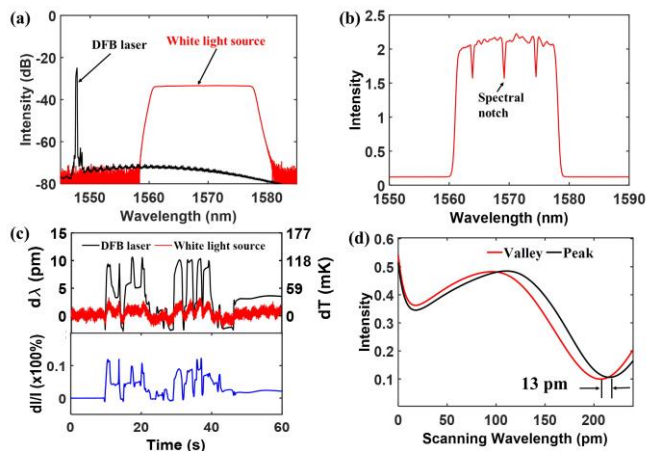


Fig. 3. (a) Spectra of the DFB laser and the SLED white-light source after passing through the CWDM obtained by the OSA. (b) Reflection spectrum of bolometer obtained by the high-speed spectrometer. (c) Upper: FOB signals interrogated by wavelength-scanning DFB laser (black) and white-light system (red) when the polarization was changed by tuning the PC; lower: DFB intensity fluctuations ( $dI/I$ ) derived from the output of the PD. (d) Normalized spectrum of the notch when it was at its shortest (red) and longest (black) wavelength positions.

As the polarization state was randomly changed by tuning the PC, the wavelength shift and equivalent relative temperature variations were interrogated from both the DFB laser and the white-light system and the results are shown in the

upper figure of Fig. 3 (c). It can be seen that response of white-light system gives a relatively small response that is synchronized with the change of the polarization, showing that the tuning the PC indeed changed the intensity of the laser injected to the FOB, which in turn varied its temperature. The laser intensity fluctuations were also obtained from the output of the PD, as shown in the lower figure in Fig. 3(c). It is seen that tuning the PC caused a maximum of 10% round-trip change of the laser intensity. The good correlation between the temperature interrogated from the white-light system and the laser intensity fluctuation further verifies that the tuning the polarization controller led to changes in laser intensity and consequent changes in FOB temperature. The wavelength shift demodulated from the DFB laser is much larger than the white-light system, indicating that the silicon FOB has a large sensitivity to the variation of the light polarization due to the birefringence of silicon FPI. To quantify the birefringence of the FOB, the PC was tuned with an attempt to cover all possible polarization states. Fig. 3(d) shows the two extreme cases where the resonant notch being monitored was at its shortest and longest positions with a wavelength separation of  $\Delta\lambda = 13$  pm. Ignoring the temperature variations resulting from the intensity changes of the DFB laser light, these cases were obtained when the laser light was linearly polarized and the polarization was aligned with each of the two principle axes of birefringence. The wavelength separation of 13 pm, corresponds to a birefringence of  $\Delta n = n_x - n_y = n\Delta\lambda/\lambda = 3.0 \times 10^{-5}$ , where  $n_x$  and  $n_y$  are the refractive indices along the two principle axes of the FOB,  $n = 3.48$  is the refractive index of silicon, and  $\lambda$  is optical wavelength of operation. This wavelength separation is equivalent to a temperature change of  $\sim 150$  mK. Note that the experimental setup shown in Fig. 2 is intended only for the study of the birefringence of the FOB and the setup for measurement of plasma radiation is different and is shown in Fig. 5 below.

### C. FOB Sensitivity to Small Polarization Variations

In many cases, laser polarization changes over a small range and the response of the FOB to polarization fluctuations is complicated. It is dependent on the exact polarization state of the light arriving at the FOB as well as how the polarization state is changed. In this section, we will consider a simple case where the light arriving at the FOB is linearly polarized at an angle of  $\theta$  with respect to the slow axis of the FOB, as shown in Fig. 4(a), and the perturbation to the polarization state is to cause a small rotation of the polarization direction. The measured reflection spectrum of the FOB is the superposition of the reflection spectra measured by the light at the two

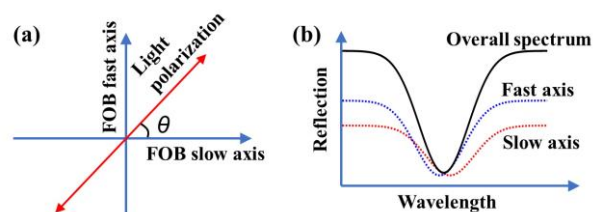


Fig. 4. (a) Light polarization with respect to the principle axes of the FOB; (b) Illustration of the measured FOB spectrum, which is a superposition of the spectra measured by the fast- and slow-axis components of the light.

principle axes of the FOB, as shown in Fig. 4(b). The spectra around the vicinity of the notch positions can be approximated by two quadratic functions, and, assuming the separation of the spectral notches caused by the FOB birefringence,  $\Delta\lambda$ , is much smaller than the width of the spectral notch, the overall reflection spectrum can be written as

$$R(\lambda) = I_0 p \left[ \cos^2 \theta \left( \lambda - \frac{\Delta\lambda}{2} \right)^2 + \sin^2 \theta \left( \lambda + \frac{\Delta\lambda}{2} \right)^2 \right], \quad (1)$$

where  $I_0$  is the overall intensity of the light arriving at the FOB and  $p$  is the fitting coefficient for the quadrature functions. Solving  $\partial R / \partial \lambda = 0$ , we obtain the wavelength position of the measured spectral notch,  $\lambda_0$ , which is given by

$$\lambda_0 = \frac{1}{2} \cos 2\theta \Delta\lambda. \quad (2)$$

Then the sensitivity of the FOB to polarization perturbations, in terms of the wavelength shift of the spectral notch caused by a unit angle of the linear polarization rotation, is given by

$$\frac{\partial \lambda_0}{\partial \theta} = -\sin 2\theta \Delta\lambda. \quad (3)$$

It is seen that the sensitivity to polarization perturbation vanishes when the polarization of the light arriving at the FOB is aligned with one of the principle axes of the FOB ( $\theta = 0^\circ$  or  $90^\circ$ ) and assumes the maximal value when the polarization is at  $45^\circ$  with respect to one of the principle axes. However, in practical applications, it may be challenging to pin the polarization of the light at the FOB to a particular state because fiber bending and rotation as well as temperature variations may cause a large change in the polarization state.

### III. INFLUENCE OF VIBRATION AND MAGNETIC FIELD APPLIED ON THE FIBER ON FOB OPERATION

In practical plasma applications, the mechanical vibration and the strong static or quasi-static magnetic field can be present in a magnetic-confinement fusion system. Interferometry measurements on tokamaks have required the use of multi-wavelength approaches to remove mechanical vibrations, and have demonstrated movements of up to 1 cm on double-pass systems at frequencies of a few Hz [11, 12]. During disruptions, tokamaks can also experience large amplitude oscillations [13]. How these macroscopic movements of the MCF device correspond to small scale oscillations for measurement systems depends on detailed design, but the potential for signal pollution is high. The optical fiber bending resulting from the mechanical vibration can induce linear birefringence, which can change the polarization of light that guided in the optical fiber. The magnetic field in the magnetic-confinement fusion systems could be static or evolving slowly over time, as well as have low amplitude,  $\delta B/B < 0.1$  high frequency,  $> 100$  kHz, components discussed in more detail later. Based on applications, the quasi-static magnetic flux density can range from approximately 1 to 12 T, depending on device and location within the torus, inducing a circular birefringence to the fiber and the silicon FPI and a Faraday rotation to the polarization of the light guided in the optical fiber and silicon FPI [14]. As shown in Section II.B, the FOB is sensitive to the light polarization due to the birefringence of silicon FPI. Both the

mechanical vibration and the dc or quasi-dc magnetic field can cause polarization variations. In this section, we experimentally study the influences of mechanical vibration and quasi-dc magnetic field on the FOB operation.

#### A. Experimental Setup

The experimental setup to characterize both the mechanical vibration and magnetic field is schematically shown in Fig. 5. This is similar to the setup that will be used for plasma radiation measurement in practical application. A different DFB diode laser with a larger wavelength scanning range was used for the demodulation operating with a same method that demonstrated in the previous section. A triangle wave with frequency of 2 kHz was used to modulate the DFB laser. In this case, the scanning wavelength range was 600 pm.

Besides the radiation, ambient temperature variations as well as laser drift will also cause responses to the bolometer. In order to remove these noises, we constructed a reference bolometer (RB) that is placed close to the sensing bolometer (SB) but shielded from the radiation. A portion of the light from the diode laser is split out via a fiber-optical coupler with a couple ratio of 33/67 and delivered to the reference bolometer. Laser wavelength drift and ambient temperature variations cause equal contributions to the responses of both bolometers. Therefore, the difference between the wavelength positions of the SB and the RB removes the common noises and only contains the information from the radiation-induced temperature rise. For either the SB or the RB, the returned light was directed to a PD and recorded by the data acquisition (DAQ) system with a sampling rate of 2 MHz. In this way, the FOB mirrors the traditional RB [2] that arranges sensing and reference bolometers a Wheatstone bridge to remove environmental noise and demodulates an AC bridge drive to achieve high signal to noise.

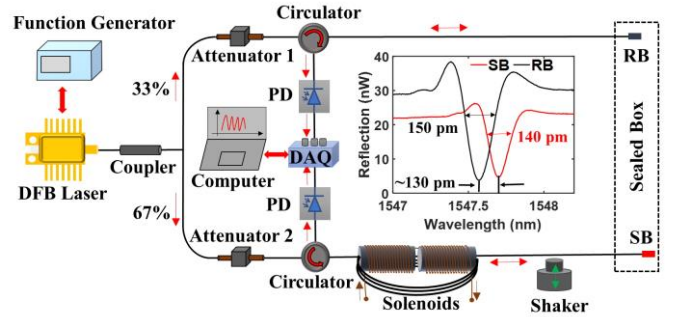


Fig. 5. Experimental setup to characterize noise performance of the FOB system. The inset shows the reflection spectral notches of the SB and the RB at room temperature.

As discussed early, the FOBs were sensitive to the power of the light injected to the FOBs due to the absorption of the gold coating. We introduced two attenuators that allowed us to conveniently fine-tune the relative positions of the resonant wavelengths of the two FBIs. The reflection spectra of the two FOBs are shown in the inset of Fig. 4 and the resonant notches were separated by  $\sim 130$  pm, which is well within the scanning range (600 pm) of the DFB laser.

For mechanical vibration testing, vibration was applied to the lead-in SMF of the SB by attaching the fiber on an

electromagnetic shaker. For magnetic field testing, a solenoid was used to generate magnetic field and a few turns of the lead-in SMF of the SB was threaded into the air-core of a solenoid so that the magnetic field was applied along the axial direction of the fiber. More details of the test conditions are provided below.

### B. Mechanical Vibration

For the mechanical vibration test, we induced a 5 Hz vibration with a peak-to-peak displacement of  $\sim 0.5$  cm to the fiber using the electromagnetic shaker. The shaker was turned on at  $t = 6$  s and remained on until  $t = 25$  s when it was turned off. During the process, the measured differential wavelength shift and the equivalent temperature change are shown in Fig. 6. Significant variations in the signal were observed between 6 – 25 s when the vibrator was on. The standard deviations (std) of the signal under vibration (6 - 25 s) are 0.066  $\mu\text{m}$  and 0.78 mK in terms of wavelength shift and equivalent temperature change, respectively. Without vibration (1-5s and 26 - 40 s), these values are, respectively, 0.014  $\mu\text{m}$  and 0.16 mK. It is seen that the vibration increased the noise of the FOB system by  $\sim 5$  times. A close-up view of the signal under vibration is shown in the inset of Fig. 6 and reveals that the variation had an oscillation pattern with the same frequency (5 Hz) of the vibration.

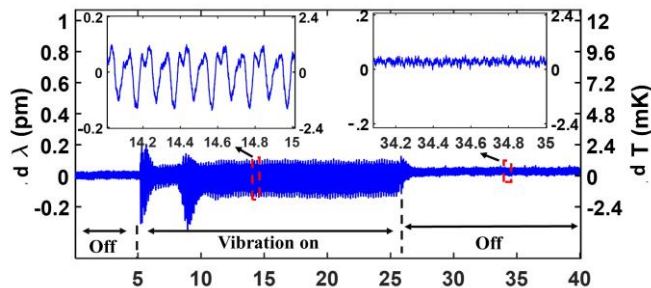


Fig. 6. FOB response to 5-Hz vibration applied on the lead-in SMF of the FOB induced by an electromagnetic shaker. The insets are the enlarged view of the signals when the shaker was on (left) and off (right).

### C. Magnetic Field

To study its effect on the FOB with a regular SMF, we placed several loops of the optical fiber with a total length of 1.1 m was placed in the air-core of a solenoid that generated a maximum of 0.05 T magnetic field at the center of the core (measured by a gaussmeter). The expected Faraday rotation from the magnetic field over this length of fiber is  $1.7^\circ$ . The solenoid was alternately turned on and off at every 10 s and the response of the FOB is shown in Fig. 7. It shows that the 0.05 T magnetic field caused a wavelength shift of 0.15  $\mu\text{m}$ , equivalent to a temperature change of  $\sim 1.8$  mK of the FOB, which is  $\sim 11$  times larger than the noise of the FOB obtained in quiet magnetic-field-free conditions (0.014  $\mu\text{m}$  or 0.16 mK). Note that, in addition to the step changes in response to the magnetic field, the FOB signal appears to have a low-frequency drift over the 50 s time span of test. Such drift was also observed in other experiments described later. The exact origins of the drift are unknown. A possible mechanism responsible for the drift is the

change of the laser heating due to the intensity variations of the DFB laser. Nevertheless, the FOB is useful for short pulse operation of MCF applications where the plasma radiation only lasts a few milliseconds and the slow drift of the FOB signal can be effectively filtered out.

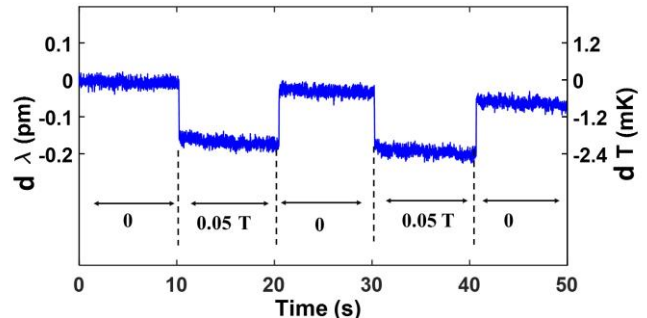


Fig. 7. FOB response to magnetic field of 0.05 T and frequency modulated by a square wave of 0.1 Hz.

Finally, we note that the polarization state of the light arriving at the FOB was not controlled. From Section II.C, the sensitivity of the FOB to polarization perturbations is dependent on the specific polarization state and specific perturbations. As a result, the responses of the FOB to vibration and magnetic field could be different at different polarization state. Nevertheless, the results show that both mechanical vibration and magnetic field can cause significant noise increase or measurement errors due to the birefringence of the FOB head and it is important to mitigate these effects for practical applications of the FOB.

## IV. MITIGATION OF BIREFRINGENCE EFFECTS

In this section we demonstrate two effective methods to mitigate the birefringence effects. The first is to use PM fiber in the FOB system and the second is to use a polarization scrambler to randomize the polarization of light from the laser source.

### A. FOB system with PM lead-in fiber

We fabricated two new FOBs with PM lead-in fibers and replaced the FOBs with the regular SMF in the FOB system shown in Fig. 5. In fabricating the FOB, the principle axes of the PM fiber were aligned with the principle axes of the FOB at an arbitrary angle. The inset in Fig. 8 (a) shows the reflection spectra of these two FOBs with PM fibers and the spectral widths are 130 and 160  $\mu\text{m}$  for the SB and RB, respectively.

For mechanical vibration test, only the PM fiber was placed on the shaker and vibrated. The mitigation of birefringence effect was characterized by using these PM bolometers without changing any other devices. PM fibers have large linear birefringence by design to prevent the coupling of the two principle linear polarization states so that the polarization of the light is maintained in the fiber even when the fiber is subject to mechanical perturbation. Indeed, the signal from the bolometer constructed on PM fibers did not show any observable changes when the vibration was turned on, as shown in Fig. 8(a).

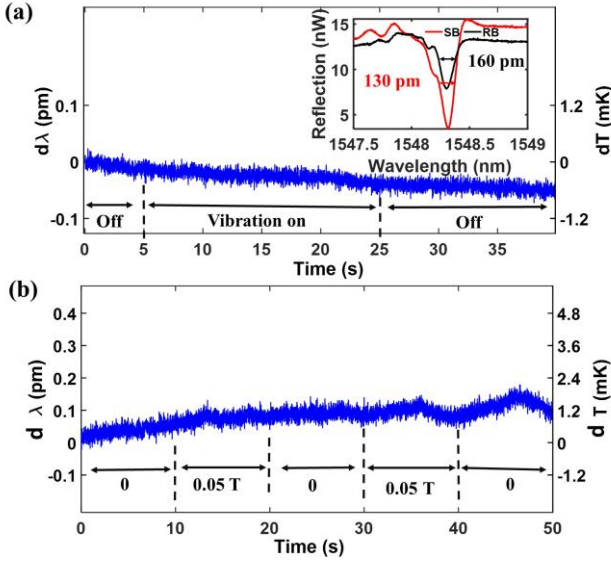


Fig. 8. PM-FOB response to vibration (a) and the magnetic field (b). The inset of (a) shows the reflection spectra the sensing bolometer and reference bolometer at room temperature.

Similar to vibration, the effect from Faraday rotation can be greatly suppressed using a PM fiber. For a PM fiber, the circular birefringence induced from the magnetic field is swamped by the much higher linear birefringence of the PM fiber. In general, the effective length that Faraday rotation can accumulate is roughly half of the beat length of the fiber [15]. While the beat-length of regular SMF can reach 10 m at the wavelength of 1550 nm [16], it is  $< 5$  mm at 1550 nm for the PM fiber used here, representing a three-orders of magnitude reduction on the effective interaction length between the fiber and the magnetic field. We then tested the FOB with a PM fiber pigtail of the same length in the field and repeated the experiment described in Section III.C. The result is shown in Fig. 8(b). Clearly, under the current system resolution, no changes were observed by the presence of the 0.05 T magnetic field.

We note that the PM fiber was only applied to the FOB pigtail, which is sufficient for the purpose of demonstration, and SMF fiber were still used for other component in the system. The FOB system would be still sensitive to vibrations and magnetic field applied on the other components with regular SMFs. In practical applications, all fibers in the system needs to be replaced with PM fibers.

### B. Polarization Scrambling

This method aims at randomizing the polarization state of the light emitted from the DFB laser using a polarization scrambler at a speed much higher than the scanning speed of the laser. As a result, each spectral frame measured by the scanning laser is the average of results from all generated random polarization states and is independent on the polarization state of the DFB diode laser. Here, a polarization scrambler (Model: PS3000, FiberPro) with a modulation frequency of 1 MHz was used to randomize the scanning laser before the light directed into the coupler. We repeated the vibration test and magnetic field test described in Sections III.B and III.C. Note that regular SMF

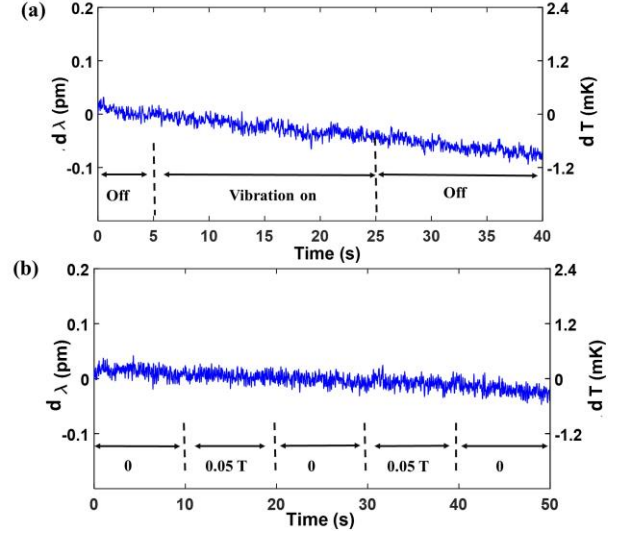


Fig. 9. FOB response to vibration (a) and magnetic field (b) after using a polarization scrambler.

was used throughout the FOB system. Figure 9(a) shows the output of the FOB system when vibration with frequency of 5 Hz was applied to the SB between 6 - 25 s. No extra noise was induced due to the vibration. Figure 9(b) is the result when the pigtail fiber of SB was exposed to a magnetic field of 0.05 T modulated by a 0.1 Hz square waveform. It is seen that the FOB system shows unmeasurable sensitivity to the magnetic field.

### C. Comparison of PM FOB and Polarization Scrambling

In our experiment, both the use of PM fibers and the polarization scrambler showed promising ability to mitigate the birefringence effects of the FOB. The PM fiber relies on maintaining a linear polarization state of the light throughout the system. The polarization extinction ratio of PM fibers may be reduced with increased fiber length and/or severe environmental perturbations. Compare with the PM FOB, the polarization scrambler randomizes the polarization states of the light in regular SMFs that can cover the whole Poincare sphere, which may make the system more resilient to environmental perturbations. However, effectiveness of the polarization scrambler in this application is dependent on the scrambling speed and the maximum modulation frequency of commercial polarization scramblers is typically limited to a few MHz. For an FOB system with high measurement speed, polarization scrambling may not be suitable. Inductive sensors close to the plasma have observed fast magnetic field fluctuations of order the 10's of mT, which could be aliased with a high-speed polarization scrambling. In NSTX-U, sustained ion-cyclotron emission was observed up to 5 MHz with  $\partial B/B$  of a few percent [17] and stronger intermittent poloidal magnetic field fluctuations prior to edge localized modes have been observed on many devices in the 10's to 100's of kHz range [18]. While these signals will fall off quickly moving away from the plasma, while line-integrated emission seen by bolometry will not, a polarization scrambling solution may still be acceptable if for some reason a PM FOB encounters other problems when testing integration into MCF systems.

## V. EFFECT OF VIBRATION AND MAGNETIC FIELD APPLIED ON FOB HEAD

Note that the vibration and magnetic field were only applied to the optical fibers of the FOB system, but not on the silicon pillar that forms the FOB head. The small size of the silicon pillar and the fact that it is directly attached to the end face of a pigtail fiber makes it difficult to apply vibration and magnetic field exclusively on the silicon FPI. Nevertheless, a brief discussion on this matter should be worthwhile.

The vibration is unlikely to cause significant bending to the silicon pillar because the small size and the cantilever configuration of the FOB head. Consequently, vibration of the silicon pillar is not expected to significantly change the polarization state of the light traveling in the silicon pillar and cause degradation in the signal. However, the effect of magnetic field applied on the silicon pillar needs more careful consideration because of the relatively large Faraday effect of silicon with a Verdet constant  $\sim 40$  times larger than that of fused silica at 1550 nm [19, 20]. Magnetic field applied on a material will induce circular birefringence to the material, which can be expressed as

$$\Delta n_c = n_+ - n_- = \nu B \lambda / \pi, \quad (4)$$

where  $n_+$  and  $n_-$  are, respectively, the refractive index for the right- and left-circular polarizations in the material,  $\nu$  is the Verdet constant,  $B$  is the magnetic field, and  $\lambda$  is the light wavelength. Using  $\nu = 0.24 \text{ rad}/(\text{T}\cdot\text{cm})$  for single-crystal silicon at  $\lambda = 1550 \text{ nm}$  [19], we estimate that the maximum magnetic field obtained in the lab  $B = 0.05 \text{ T}$  would yields a circular birefringence of  $\Delta n_c = 5.9 \times 10^{-7}$ . This is 50 times smaller than the measured value of the linear birefringence of the FOB head (see Section II.B). As a result, its effect on the measurement is likely unobservable under the test conditions in this study. It is worth noting that, in practical MCF applications with magnetic field that can reach  $\sim 12 \text{ T}$ , the induced circular birefringence may become comparable to or even exceed the linear birefringence. The two mitigation methods studied here for the linear birefringence of the silicon pillar should be equally effective for the circular birefringence.

## VI. CONCLUSION

The advantages of fiber-optics sensing technique motivated us to develop a new FOB to overcome the limitations of the resistive bolometer. Based on a previously demonstrated FOB, we studied the influences of mechanical vibration and magnetic field on the performance of FOBs and the mitigation of the influences. First, we characterized the birefringence of the FOB. The experimental results showed that the FOB had a high sensitivity to the light polarization variation due to the birefringence of the silicon FPI. Then we characterized the FOB performance of both mechanical vibration and magnetic field that can be presented in the practical plasma applications. Both mechanical vibration and magnetic field contribute to the variation of polarization of the light guided in the fiber, which, in turn, increase the noise of the FOB system. The experimental results showed that both the mechanical vibration and magnetic field introduce large noise to the performance of FOB. To mitigate the birefringence effects, two methods were studied: using PM fiber for FOB system and using a polarization

scrambler after the laser source. The experimental results show that these methods can effectively mitigate the birefringence effects of the silicon FPI. These results show that the FOB is a promising technology for plasma diagnosis in magnetic confinement fusion systems. We also note that, due to limitation of the experimental set up in our laboratory and the complexity of the fusion systems, it is difficult to accurately simulate the vibration and magnetic field in fusion systems. Further development is needed and underway before the bolometer can be tested in fusion systems in practice.

## REFERENCES

- [1] J. Ongena, R. Koch, R. Wolf, and H. Zohm, "Magnetic-confinement fusion," *Nat. Phys.*, vol. 12, p. 398, May 2016.
- [2] K. F. Mast, J. C. Vallet, C. Andelfinger, P. Betzler, H. Kraus, and G. Schramm, "A low noise highly integrated bolometer array for absolute measurement of VUV and soft x radiation," *Rev. Sci. Instrum.*, vol. 62, no. 3, pp. 744-750, 1991.
- [3] H. Meister, M. Willmeroth, D. Zhang, A. Gottwald, M. Krumrey, and F. Scholze, "Broad-band efficiency calibration of ITER bolometer prototypes using Pt absorbers on SiN membranes," *Rev. Sci. Instrum.*, vol. 84, no. 12, p. 123501, 2013.
- [4] B. J. Peterson *et al.*, "Development of imaging bolometers for magnetic fusion reactors (invited)," *Rev. Sci. Instrum.*, vol. 79, no. 10, p. 10E301, 2008.
- [5] Q. Sheng, G. Liu, M. L. Reinke, and M. Han, "A fiber-optic bolometer based on a high-finesse silicon Fabry-Pérot interferometer," *Rev. Sci. Instrum.*, vol. 89, no. 6, p. 065002, 2018.
- [6] M. L. Reinke *et al.*, "Development of plasma bolometers using fiber-optic temperature sensors," *Rev. Sci. Instrum.*, vol. 87, no. 11, p. 11E708, 2016.
- [7] G. Liu, Q. Sheng, W. Hou, M. L. Reinke, and M. Han, "A Silicon-tipped Fiber-optic Sensing Platform with High Resolution and Fast Response," *JoVE*, no. 143, p. e59026, Jan. 2019.
- [8] Y. H. Meyer, "Fringe shape with an interferential wedge," *J. Opt. Soc. Am.*, vol. 71, no. 10, pp. 1255-1263, Oct. 1981.
- [9] S. Lederhandler, "Infrared studies of birefringence in silicon," *J. Appl. Phys.*, vol. 30, no. 11, pp. 1631-1638, 1959.
- [10] G. Liu, M. Han, and W. Hou, "High-resolution and fast-response fiber-optic temperature sensor using silicon Fabry-Pérot cavity," *Opt. Express*, vol. 23, no. 6, pp. 7237-7247, Mar. 2015.
- [11] T. N. Carlstrom, D. R. Ahlgren, and J. Crosbie, "Real - time, vibration - compensated CO2 interferometer operation on the DIII - D tokamak," *Rev. Sci. Instrum.*, vol. 59, no. 7, pp. 1063-1066, 1988.
- [12] W. F. Bergerson, P. Xu, J. H. Irby, D. L. Brower, W. X. Ding, and E. S. Marmor, "Far-infrared polarimetry diagnostic for measurement of internal magnetic field dynamics and fluctuations in the C-MOD Tokamak (invited)," *Rev. Sci. Instrum.*, vol. 83, no. 10, p. 10E316, 2012.
- [13] V. Riccardo, "Chapter 7: Disruption Studies in JET," *Fus. Sci. Technol.*, vol. 53, no. 4, pp. 1064-1079, May 2008.
- [14] A. M. Smith, "Polarization and magneto-optic properties of single-mode optical fiber," *Appl. Opt.*, vol. 17, no. 1, pp. 52-56, Jan. 1978.
- [15] R. I. Laming and D. N. Payne, "Electric current sensors employing spun highly birefringent optical fibers," *J. Lightwave Technol.*, vol. 7, no. 12, pp. 2084-2094, 1989.
- [16] S. Xie, X. Bao, and L. Chen, *Distributed fiber beat length, birefringence and differential group delay measurement using BOTDA technique* (21st International Conference on Optical Fibre Sensors (OFS21)). SPIE, 2011.
- [17] E. D. Fredrickson *et al.*, "Emission in the ion cyclotron range of frequencies (ICE) on NSTX and NSTX-U," *Phys. Plasmas*, vol. 26, no. 3, p. 032111, 2019.
- [18] F. M. Laggner, A. Diallo, M. Cavedon, and E. Kolemen, "Inter-ELM pedestal localized fluctuations in tokamaks: Summary of multi-machine observations," *Nuclear Mater. Energy*, vol. 19, pp. 479-486, May 2019.
- [19] H. Piller and R. F. Potter, "Faraday Rotation Near the Band Edge of Silicon," *Phys. Rev. Lett.*, vol. 9, no. 5, pp. 203-205, Sep. 1962.
- [20] J. Noda, T. Hosaka, Y. Sasaki, and R. Ulrich, "Dispersion of Verdet constant in stress-birefringent silica fibre," *Electron. Lett.*, vol. 20, no. 22, pp. 906-908, 1984.